M. Hossain, C. Telke, M. Sparing, A. Abdkader, A. Nocke, R. Unger, G. Fuchs, A. Berger, C. Cherif, M. Beitelschmidt, L. Schultz

Mathematical modeling, simulation and validation of the dynamic yarn path in a superconducting magnet bearing (SMB) ring spinning system

Erstveröffentlichung in / First published in:

Textile Research Journal. 2017, 87(8), S. 1011 – 1022 *[Zugriff am: 07.08.2019]*. SAGE journals. ISSN 1746-7748.

DOI: https://doi.org/10.1177/0040517516641363

Textile Research Journal

Review article

Textile Research Journal
2017, Vol. 87(8) 1011–1022

DOI: 10.1177/0040517516641363
journals.sagepub.com/home/trj
SAGE

Mathematical modeling, simulation and validation of the dynamic yarn path in a superconducting magnet bearing (SMB) ring spinning system

M Hossain[1], C Telke[2], M Sparing[3], A Abdkader[1], A Nocke[1], R Unger[1], G Fuchs[3], A Berger[3], C Cherif[1], M Beitelschmidt[2] and L Schultz[3]

Abstract

The new concept of a superconducting magnetic bearing (SMB) system can be implemented as a twisting element instead of the existing one in a ring spinning machine, thus overcoming one of its main frictional limitations. In the SMB, a permanent magnet (PM) ring rotates freely above the superconducting ring due to the levitation forces. The revolution of the PM ring imparts twists similarly to the traveler in the existing twisting system. In this paper, the forces acting on the dynamic yarn path resulting from this new technology are investigated and described with a mathematical model. The equation of yarn movement between the delivery rollers and the PM ring is integrated with the Runge-Kutta method using MATLAB. Thus, the developed model can estimate the yarn tension and balloon form according to different spindle speeds considering the dynamic behavior of the permanent magnet of the SMB system. To validate the model, the important relevant process parameters, such as the yarn tension, are measured at different regions of the yarn path, and the balloon forms are recorded during spinning with the SMB system using a high speed camera.

Keywords

mathematical modeling, yarn tension, balloon form, ring spinning, superconducting magnetic bearing

In the existing ring spinning process, the frictional heat generated in the ring/traveler system causes damage to both the twisting element and the yarn structure.[1] The traveler is not allowed to rotate at more than 50 m/s, especially in the case of man-made fibers, due to their melting, caused by the high friction-induced heating, which limits productivity.[2,3] The friction-free superconducting magnet bearing (SMB) eliminates this restriction and thus allows increase of the spindle speed much higher than with existing spinning machines. In our previous work, different concepts of SMB system have been presented, and a suitable one has been successfully integrated in a ring spinning tester.[4] The SMB system comprises of two rings, a magnetic element of Neodymium Iron Boron (NdFeB) with a yarn guide attached to it, and a high temperature superconductor (SC) from YBCO ($YBa_2Cu_3O_{7-x}$) chemical compounds. The superconductor (SC) ring is cooled down below its critical temperature at a fixed distance from the PM ring. The PM ring levitates above the SC ring according to the principle of levitation. During the spinning process, the yarn (wound onto the bobbin) rotates the PM ring, instead of the traveler. The patented concept of the SMB system ensures a smooth running of the spinning process for significantly higher productivity with similar yarn properties to the conventional process.[5]

[1]Institute of Textile Machinery and High Performance Material Technology (ITM), Technische Universität Dresden, Dresden, Germany
[2]Chair of Dynamics and Mechanism Design, Institute of Solid Mechanics, Technische Universität Dresden, Dresden, Germany
[3]IFW Dresden, Institute for Metallic Materials, Dresden, Germany

Corresponding author:
M Hossain, Institute of Textile Machinery and High Performance Material Technology (ITM), Technische Universität Dresden, Hohe Straße 6, Dresden 01069, Germany.
Email: mahmud.hossain@tu-dresden.de

However, more investigations are necessary to analyze the physical challenges of the new technology during the spinning process. The research work is based on the dynamic behavior of the novel SMB system for the ring spinning process, which is a combination of textile and superconducting technology, and describes the theoretical modeling, simulation, and measurement methods for the dynamic yarn path with this magnetic bearing. The dynamic yarn path and the resultant forces of the SMB system are theoretically modeled with respect to spindle speed, yarn count, balloon geometry, and the mass and diameter of the PM ring. In the numerical solution, the boundary conditions of the yarn path with the SMB system are also described. This model provides information about the dynamical forces during the spinning process and helps to determine the textile technological and physical limitation for SMB system. Furthermore, the calculated yarn tension and corresponding balloon form from this developed model help to evaluate the new system, especially at higher spindle speed.

Theoretical model

There are many theoretical models for the prediction of the balloon form and its associated yarn tension.[6–22] Crank described the balloon in a quasi-stationary case in cap spinning, considering the centrifugal, Coriolis, and gravitational forces.[6] Mack neglected the Coriolis forces in the equation of motion of yarn, and considered the air drag constant related to the Reynold's number.[7] He described the equation in non-dimensional form and introduced the inextensibility condition. However, the boundary condition of the equation was not clearly shown in his work. De Barr showed how the yarn tension depends on process parameters, such as the friction between ring and traveler, air drag, balloon form, etc. He also applied the modeling to the balloon considering the balloon control ring.[8–11] Lisini described the balloon dynamics as a two point boundary value problem and presented the equation of motion in the ring spinning process in both the stationary and non-stationary cases.[12] Batra solved the non-dimensional equations by integrating the dynamics of traveler using the Runge-Kutta method.[13–16] Fraser explored the relationship between guide eye tension and traveler mass, mainly in the case of free balloon spinning.[17] He solved the equations numerically in a dimensionless form to avoid the complexity of several influencing parameters, such as the spindle speed. Recently, we have described the equation of motion in dimensioned form, considering the Coriolis force, and have solved the equation numerically to discover the actual yarn tension and balloon form in non-normalized values with respect to spindle speed for the conventional ring spinning system, which is significant compared to other existing models.[23] Moreover, the developed algorithm of sensitivity analysis provides a solution space with valid stable initial values for the numerical solution, as the equation of motion is highly non-linear. The simulated results, such as the yarn tension and the balloon forms, have also been validated with the measured values. In the new ring spinning method, the existing ring/traveler system has been replaced by the SMB system, which changes the yarn tension distribution and balloon geometry during the spinning process. That is why the existing model of ring/traveler system and the dynamical yarn path need to be described afresh, especially for the yarn path in regions III and IV (Figure 1). In this paper, the theoretical model described in Hossain et al.[23] is modified considering the dynamics of the SMB system in the ring spinning process.

For this purpose, at first the dynamics of the rotating PM ring during the spinning process have been theoretically modeled. The mathematical modeling of the yarn path between the delivery rollers and the PM ring is similar to that of the conventional one. However, the boundary conditions for the numerical solutions derived from the equation of the PM ring are described in the section below.

Equation of motion of the permanent magnet (PM) in the SMB system

The attainable bearing force, $\boldsymbol{F_B}$, in the SMB system is based on the flux pinning of magnetic fluxes penetrating the superconductor, obtained after field-cooling the superconducting ring, and can be expressed as[24]

$$\boldsymbol{F_B} \sim B^* \text{grad } \mathbf{B}\, \mathrm{d}V \tag{1}$$

This means that the achievable bearing force is proportional to the maximum flux density, B^*, and the gradient of the field change in the superconductor. The field distribution of PM rings is arranged in a way that high values of B^* and grad$\mathbf{B}$ can be achieved in the largest possible volume of the superconductor (SC). If the SC is deflected in the SMB system, an attractive or repulsive force acts to hold the PM in its original position.[25]

The SMB system is mathematically described as a spring–mass–damper system, in which the PM ring is driven by the spindle via the yarn attached to it. The yarn tension acting at the yarn guide of the PM ring can be described with the help of Figure 1(b). T_1 and T_2 are the yarn tensions at the yarn guide of the PM ring on the balloon side and on the cop side, respectively. The total yarn tension, T_G, that is, the sum of the yarn tensions T_1 and T_2, results in the radial, axial, and tilt displacement of the PM ring. This displacement is

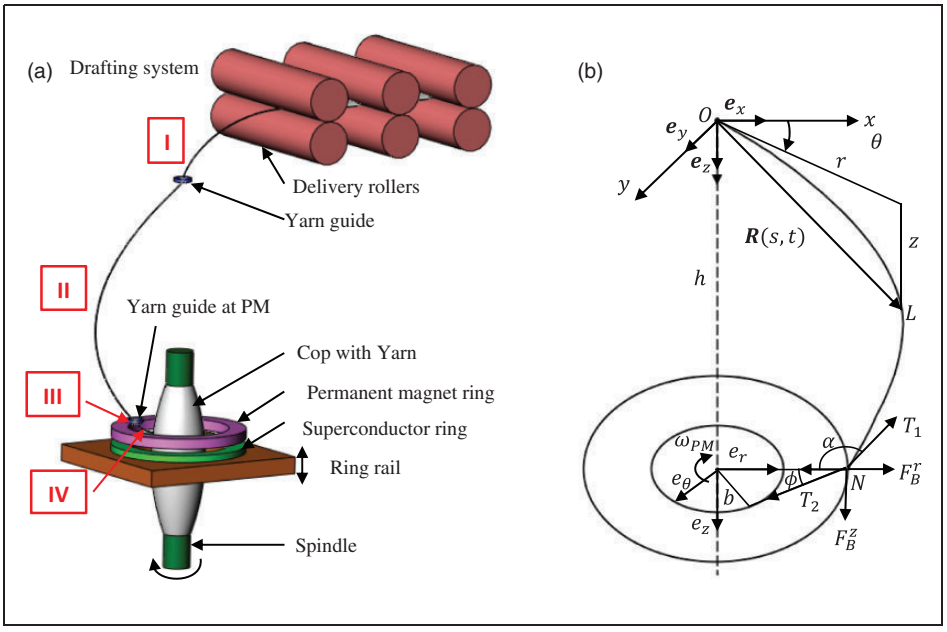

Figure 1. The ring spinning process with a superconducting magnetic bearing (SMB). (a) Schematic diagram of spinning and definition of yarn path at different regions[23]: I—between delivery rollers and yarn guide; II—between yarn guide and yarn guide at PM; III—through yarn guide of PM; IV—between yarn guide of PM and cop. (b) Definition of coordinate systems and yarn path.

counteracted by the strong restoring forces of the SMB system—F_B^z in the axial, and F_B in the radial directions. There exists no restoring force in the circumferential direction for this round SMB geometry, thus the total external yarn tension, T_G^θ, in the circumferential direction acts as a driving force for the free rotation of the PM ring. The amplitudes of displacement for the different directions of yarn forces are defined by the bearing stiffness.[25]

The rotation of the PM ring is thus described in equation (2), according to the principle of angular momentum

$$\dot{\omega}_{PM} J_R + d_R \omega_{PM} = T_G^\theta(t) a_{iPM} \tag{2}$$

where ω_{PM} is the angular velocity of the PM ring, $\dot{\omega}_{PM} \equiv d(\omega_{PM})/dt$, J_R is the moment of inertia, d_R is the damping constant of rotation of the rotating PM ring, and a_{iPM} is the inner radius of the PM ring. Air friction and dissipative processes in the superconductor damp the rotation of the PM ring. For the quasi-stationary case, the angular acceleration of the PM ring is $\dot{\omega}_{PM} = 0$ and, therefore, equation (2) can be written as

$$d_R \omega_{PM} = T_G^\theta a_{iPM} \tag{3}$$

The constant angular frequency of the PM ring

$$\omega_{PM} = \frac{T_G^\theta(t) a_{iPM}}{d_R}$$

is determined by equilibrium between the yarn force, T_G^θ, and the damping. This damping of the PM ring influences the motion of the ring, and is responsible for the necessary slip between spindle and ring.

In the case of free rotation without external yarn force—that is, when $T_G^\theta = 0$ (e.g. during end-breakages) equation (2) simplifies to

$$\dot{\omega}_{PM} + 2\delta_{\text{rot}} \omega_{PM} = 0 \tag{4}$$

with

$$\delta_{\text{rot}} = \frac{d_R}{2J_R} \tag{5}$$

where δ_{rot} is the decay constant of the damped oscillation of the PM ring without external forces. The yarn-driven rotational motion of the PM-ring is decelerated by air friction and the viscous motion of the flux lines (vortices) from the superconductor. This is described by the rotational decay constant, δ_{rot}, in equation (5). This constant is determined by accelerating the PM in the ring spinning machine up to the defined spindle speeds, such as 5000, 20,000, etc. The decelerations of the PM ring are measured over time from the defined spindle speed to still stand after cutting the yarn.

Mathematical formulation of the yarn path

In the mathematical description of the yarn path, the yarn is considered as a one dimensional continuum with

homogeneous and circular cross section, so that only yarn tension acts in the yarn. The other important assumptions and limitations of the presented model are as follows.

- The yarn is considered to be inextensible.
- The influences of centrifugal force and Coriolis force are considered.
- The dynamic model during synchronous running of the PM is considered.
- The friction between yarn and the yarn guide at the PM is considered constant.
- The movement of the ring rail is not considered.
- Balloon control ring is not considered.
- The effect of yarn twist is neglected.

As shown in Figure 1(a), the yarn path from the delivery roller to the winding point of the cop has been divided in four regions. The theoretical modeling of the dynamic yarn path in regions I and II is partly based on the existing mathematical models of the conventional ring spinning process,[23] which is developed taking into account the above-mentioned assumptions and conditions. The dynamic forces, such as centrifugal forces, air resistance forces, and the Coriolis force, mainly govern the geometry of the dynamic yarn path and control the tension distribution along the yarn path. In order to define the yarn path, Figure 1(b) describes a rotating cylindrical coordinate system of $r(s), \theta(s), z(s)$ corresponding to the unit vectors $\boldsymbol{e_r}, \boldsymbol{e_\theta}, \boldsymbol{e_z}$, which rotates with the angular speed of the PM ring and describes the dynamic forces. If a material point, L, is defined as position vector $\boldsymbol{R}(s,t) = r\boldsymbol{e_r} + z\boldsymbol{e_z}$, the equation of motion of yarn dynamics can be formulated as follows, according to the well-known equation of motion[17]

$$m\left\{\mathfrak{D}^2\boldsymbol{R} + 2\omega_{PM}e_z \times \mathfrak{D}\boldsymbol{R} + \omega_{PM}^2\boldsymbol{e_z} \times (\boldsymbol{e_z} \times \boldsymbol{R})\right\} = \frac{\partial}{\partial s}\left(T\frac{\partial}{\partial s}\boldsymbol{R}\right) + \boldsymbol{F} \tag{6}$$

where m is the yarn mass in g/km, ω_{PM} is the angular velocity of the PM ring, $\mathfrak{D}$ is the differential operator, and $\boldsymbol{F}$ denotes the air drag force per unit length. If the problem is considered as quasi-stationary, equation (6) can be expressed as follows, in dimensioned form

$$m\left\{v^2\frac{\mathrm{d}^2\boldsymbol{R}}{\mathrm{d}s^2} + 2\omega_{PM}v\boldsymbol{e_z} \times \frac{\mathrm{d}\boldsymbol{R}}{\mathrm{d}s} + \omega_{PM}^2\boldsymbol{e_z} \times (\boldsymbol{e_z} \times \boldsymbol{R})\right\} = T'\frac{\mathrm{d}\boldsymbol{R}}{\mathrm{d}s} + T\frac{\mathrm{d}^2\boldsymbol{R}}{\mathrm{d}s^2} + \boldsymbol{F} \tag{7}$$

where v is the delivery velocity of the yarn at the delivery rollers.

Equation (7) is a second order differential equation system for the yarn path at point L. The boundary conditions for this mathematical problem at the yarn guide of the PM ring, considering the dynamics of the PM ring, have to be defined for the numerical solution.

Boundary conditions for the numerical solution of SMB system

The first boundary condition at the yarn guide is as follows.

For the guide eye (O (Figure 1(b)), the boundary conditions are[23]

$$r(0) = 10^{-3}\mathrm{m},\ \theta(0) = 0,\ z(0) = 0 \tag{8}$$

The first boundary condition at the yarn guide of the PM ring, N, (Figure 1(b)) is

$$r(s_l) = a_{iPM}, \quad z(s_l) = h \tag{9}$$

where s_l describes the length of the yarn between yarn guide and the yarn guide of PM ring at N and h is the balloon height (Figure 1(b)).

The second boundary condition at the yarn guide of the PM ring can be defined from the equation of motion of the PM ring (equation (3)), where the left side of the equation describes the components of the yarn tension, T_1 and T_2, in the circumferential direction (Figure 1(b))

$$T_1[g\sin\phi - a_{iPM}\theta'(s_l)]a_{iPM} = d_R\omega_{PM} \tag{10}$$

where T_1 is the yarn tension at the yarn guide of the PM ring on the balloon side and $g(= e^{\mu_y\alpha} = 1.7)$ is the frictional parameter between yarn and yarn guide of the PM ring as constant, $()' \equiv d()/ds$.[17] The yarn tension at the yarn guide of the PM ring on the cop side, T_2 (Figure 1(b)), is estimated by the Euler equation, as follows

$$T_2 = T_1 \cdot e^{\mu_y\alpha} \tag{11}$$

where μ_y is the frictional coefficient between the yarn and the yarn guide of the PM ring and α is the angle shown in Figure 1(b). The frictional parameter is considered constant for this modeling, as mentioned in the assumptions. However, the new concept needs to be developed to measure the friction between the yarn and the yarn guide of the PM ring during the spinning process at different spindle speeds.

Numerical solution of the theoretical model for SMB system

The equation of motion of the yarn path described in equation (7) is integrated with the Runge-Kutta method with a spatial step size of 0.0001 using MATLAB, and optimized using a shooting method so that the above-mentioned boundary conditions (in equations (8–10) are fulfilled.[27] Finally, an iterative optimization method with the Levenberg–Marquardt algorithm is applied to minimize the squared error residual sum of the reformulated boundary conditions. The boundary conditions described in equations (9) and (10) are reformulated to obtain the residual Γ_1 and Γ_2, with the weighted function, ζ_k, as follows

$$\Gamma_1 = \zeta_1(r(s_l, T_0, r') - a_{iPM})^2 \tag{12}$$

$$\Gamma_2 = \zeta_2[T_1[e^{\mu_y \alpha} \sin\phi - a_{iPM}\theta'(s_l, T_0, r')]a_{iPM} - d_R\omega_{PM}]^2 \tag{13}$$

where T_0 is the yarn tension at the guide eye (O, as shown in Figure 1(b)), T_1 is the yarn tension at the yarn guide of the PM ring on the balloon side, ω_{PM} is the velocity of the PM ring, and ϕ the angle shown in Figure 1(b).

The sum of residual results is

$$\Gamma(s_l, T_0, r') = \sum_{i=1}^{N} \zeta_i \Gamma_i(s_l, T_0, r') \tag{14}$$

During the optimization, the start values, $T_0(0)$ and $r'(0)$, are varied so that minimum errors can be achieved in relation to the boundary conditions

$$\min_{T_0, r'} \Gamma(s_l, T_0, r') = \min_{T_0, r'} \sum_{i=1}^{N} \zeta_i \Gamma_i(s_l, T_0, r') \tag{15}$$

The parameters considered for the numerical solution and for the experiments are listed in Appendix 1. From this numerical solution, the yarn tensions are solved for regions I, II, and III. The yarn tension at region IV is calculated, considering a constant frictional parameter between the yarn and the yarn guide of the PM ring, using equation (11). The results from the numerical solution of the presented model predict the yarn tension and balloon form with different spindle speeds from 5000 to 25,000 r/min (Appendix 2 and Figure 3(a)). In Appendix 2, the yarn tension for regions I–IV and the geometry corresponding to the balloon are presented according to the different spindle speeds. The yarn tensions at all regions increase with respect to spindle speed. The balloon forms also increase due to the centrifugal forces with respect to spindle speeds from 5000 to the 20,000 r/min, which is shown in Figure 3(a). The quantitative values of maximum balloon diameter according to spindle speed are also shown in Appendix 2. As the implementation of the SMB system is aimed at spinning yarn at higher spindle speed than the existing ring traveler system, the aim of the modeling is to gather information about the changes of yarn tension and balloon forms with the new SMB system, especially considering the spindle speeds. The results can be considered for the stationary case when the yarn PM ring and spindle run synchronously.

Characterization of the developed model for SMB system

In order to characterize the dynamic yarn path and to validate the presented model, the yarn tensions are measured at different regions, such as in regions I, II, and IV (Figure 1(a)).

The goal is to measure the important physical factors influencing the yarn and SMB system, and to explore their interaction with respect to different spindle speeds. The different principles of yarn tension measurement in region I, II, and IV have already been implemented in the conventional ring spinning process with the ring/traveler system.[28] After some modifications, the sensors are further applied in the case of SMB spinning. Moreover, the balloon forms are recorded with the high speed camera at different spindle speeds.

Before the measurement of the yarn tension, the ring spinning tester available at the Institute of Textile Machinery and High Performance Material Technology (ITM), Dresden was constructively modified for the special technological requirements. The ring rail, spindle, front casing behind the spindle, etc., of the existing ring spinning tester were replaced with non-magnetic materials, so that the magnetic forces of the PM ring and the levitation forces of the SMB system were not magnetically influenced. The cryostat used for the cooling and thermal insulation of the SMB system was integrated on the ring rail of the spinning tester, as shown in Figure 2. The superconducting ring mounted in the cylindrical casing must remain cold below its transitions temperature (−196°C). For this purpose, the connection system of the casing ensures a continuous supply of liquid nitrogen (LN_2) from a cryogenic dewar with a definite pressure and flow rate of LN_2. The temperature inside the cryogenic system is continuously monitored by a thermo-element. An insulating process is maintained between the superconductor and the outer cryostat surface by constant pumping

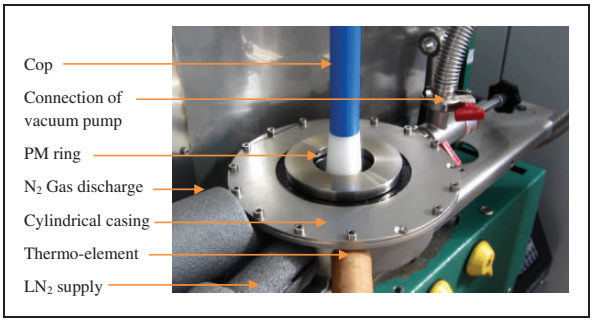

Figure 2. Integration of superconducting magnetic bearing (SMB) and cryostat in a ring spinning tester.

with a vacuum pump. To fix the initial levitation distance the PM ring is placed above the superconductor (SC), positioned with three distance pieces on the top of the cryogenic system. The PM ring is then centered with the help of a centering device with respect to the spindle. When the temperature falls to −196°C, the distance pieces are removed. The PM ring is now free to rotate over the SC, or rather on the cylinder casing, and is ready to start the spinning process with the SMB system.

Balloon form (Region II)

The recording of balloon forms is carried out by using a high speed camera (Photron Fastcam Ultima SA-3, frame rate 12.5 KHz for 1024 × 1024 pixel) at the ITM-ring spinning tester to determine the influence of centrifugal force and air resistance on the balloon form. A black reference grid is fixed behind the spindle to avoid the reflection of light during the experiment. The balloon forms are measured at spindle speeds of 5000, 10,000, 15,000, and 20,000 r/min, and at different ring rail positions, as shown in Figure 3(b). According to the Figure 3(b), the position of maximum radius of balloon is located in the plane of PM ring at lower spindle speed such as at 5000 r/min. At higher spindle speed, the maximum radius of balloon locates in the middle of the yarn guide and PM ring due to higher centrifugal force.

The recorded images of balloon form have been analyzed to measure the maximum balloon diameter using the software Image J.[29] Each maximum balloon form for a defined spindle speed has been measured several times with this program. For the measurement of balloon form with Image J, at first a straight line is drawn on the bobbin diameter of the image. The program records the x, y-coordinates and the length of the line in pixels, to define the spatial length of the active image of the balloon form in calibrated units. The scale can be set to enter the known diameter of the cop. The distance in the pixels field will be then automatically be filled in, based on the length of the line selection.

The actual diameter of the balloon can be measured similarly (Figure 4). The balloon forms are also listed for spindle speeds from 5000 to 20,000 r/min in Table 1. According to Figure 3(b) and Table 1, the balloon forms increase with respect to spindle speed.

Yarn tension between delivery rollers and yarn guide (Region I)

A three-point sensor from Tensometric Messtechnik GmbH is used for the measurement of tension in region I at different spindle speeds (Figure 5(a)).

The yarn path acting radially on the measuring roller of the sensor deforms the complex-shaped cantilever attached to it. The full bridge of built-in strain gauges converts this deformation into a proportional electrical output signal, which is recorded using LabView Signal Express. During calibration, dead weights of 10 g and 20 g are hung over the spun yarn to set the scale in the data acquisition program. The experiment is repeated in the SMB ring spinning tester to verify the measured values. The mean values of yarn tension for different spindle speeds are shown in Figure 5(b). According to Figure 5(b), yarn tension increases with higher spindle speed in both in the calculated and experimental results. The measured values are close to the calculated ones, especially at the spindle speeds of 5000 and 10,000 r/min. As the spindle speed increases further, such as at 15,000 r/min, the vibration of the PM ring causes a yarn tension increment and generates peaks, which is still more prominent at 20,000 r/min. Moreover, the twist propagation of the yarn from the PM ring to the delivery rollers is retarded by the measuring sensor, and reduces the strength of the yarn, resulting in frequent end-breakages. For this reason, measurement has not been carried out for higher speeds, such as 25,000 r/min. Modification of the sensor with the rotating guiding elements and measuring roller should solve the problem of continuous end-breakages during measurement of yarn tension.

Yarn tension between yarn guide and PM ring (Region II)

In order to measure the yarn tension in the balloon—that is, between the yarn guide and the yarn guide of the PM ring—a sensor from Tensometric GmbH, Germany, has been modified. The sensor consists of a measuring roller and two guiding rollers, which are fixed to the sensor part. The measuring roller measures the radial force of the rotating balloon acting on it, and the two guide rollers keep the yarn path deflection constant.

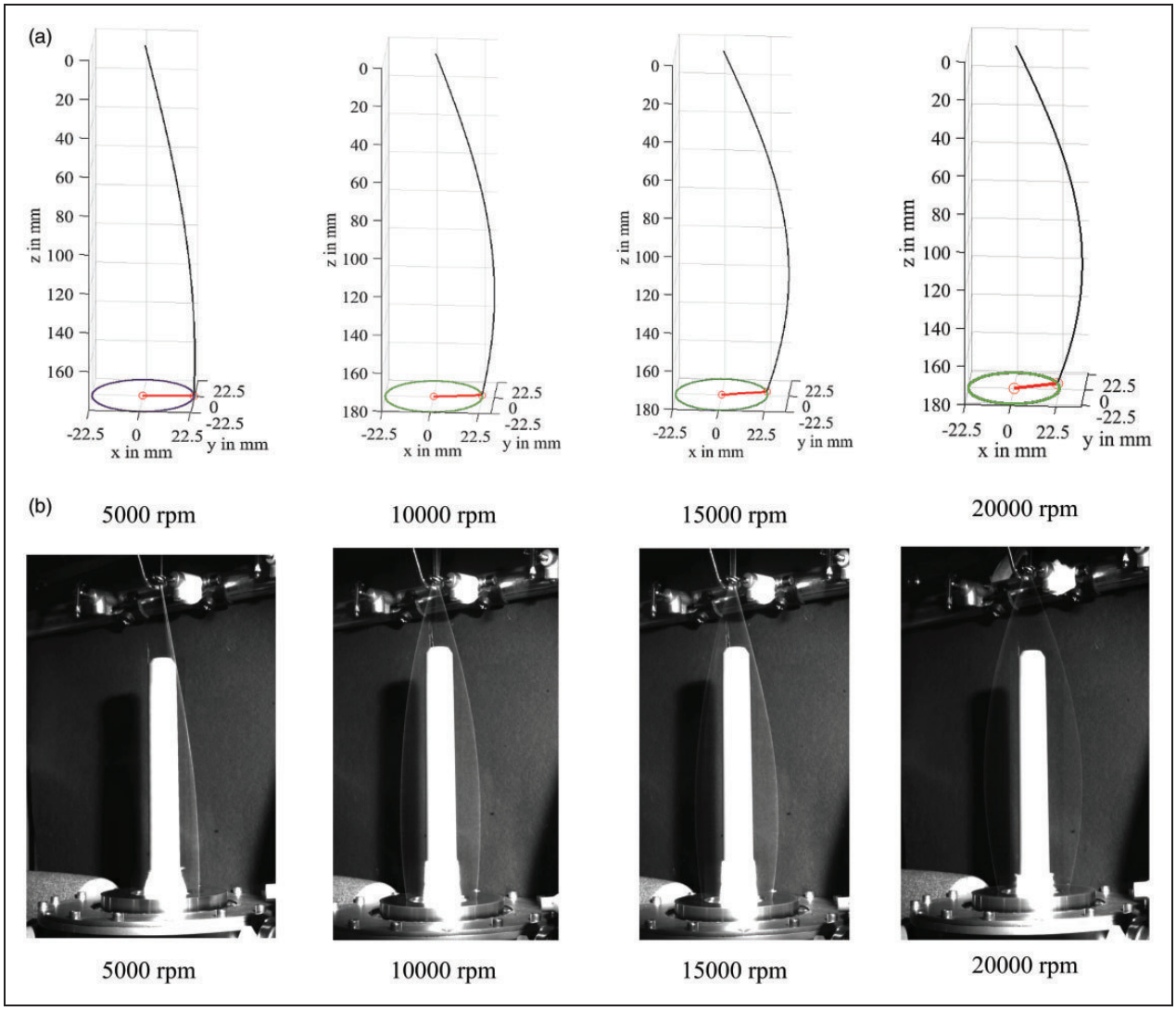

Figure 3. (a) Balloon forms from numerical results. (b) The recorded balloon forms at different spindle speeds.

During calibration of the sensor, different dead weights, such as 10 g and 20 g, are hung on the spun yarn, so that the yarn presses against the measuring roller. The corresponding yarn tension in the longitudinal direction can be measured through the radial force. The sensor is positioned in such a way that the balloon touches the measuring roller and the guiding element (Figure 6(a)). The results are recorded in a data acquisition LabView program and are analyzed with DIAdem. According to Figure 6(b), the mean value of yarn tension increases according to the spindle speed, as expected. The mean yarn tension at the spindle speeds of 5000 to 20,000 r/min are found to be from 5 cN to 55 cN, with 2% variation, respectively (Figure 6(b)). However, the balloon deforms to a certain level after touching the measuring roller of the sensor using this method, especially at higher spindle speed, which influences the measured values.

Yarn tension between the yarn guide of the PM ring and the winding point of cop (Region IV)

As shown in Figure 7(a), the measuring ring (7), which is mounted concentrically between the PM ring (5) and the cop (8), is constructed from non-magnetic material to avoid magnetic influences during measurement (Figure 7(a)). The yarn path from the yarn guide of the PM to the winding point of the cop presses against the measuring ring and deflects the spring leaves mounted under the measuring ring. Moreover, four spring leaves with strain gauges are mounted under the measuring ring. The deflection of the strain gauges attached to these leaves changes the electrical signal, which is recorded with a data acquisition program LABView Signal Express.

During the calibration, the dead weight, of 10 and 20 g are hung over the measuring ring with spun yarn,

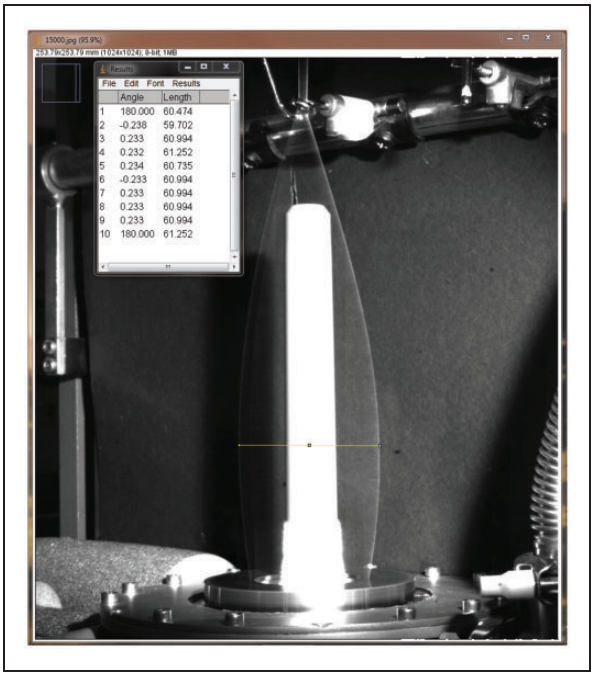

Figure 4. Measurement of maximum balloon diameter at the spindle speed of 15,000 r/min.

Table 1. Measured values of maximum balloon diameter

Spindle speed (r/min)	Mean value of diameter (mm)	Standard deviation
5000	45.7	0.2
10,000	57.5	0.3
15,000	60.8	0.3
20,000	68.7	0.4

and thus set the scale in LabView SignalExpress, accordingly. The mean values of measured yarn tension are presented in Figure 7(b) for different spindle speeds. According to Figure 7(b), the yarn tension increases with respect to spindle speed from 5000 to 20,000 r/min. However, the variation of the yarn tension during the measurements can be attributed to the dynamic friction between the rotating yarn and the measuring ring, and also due to the eccentricity of the measuring ring.

In Table 2, the mean measured yarn tensions at all yarn regions have been summarized. The highest yarn tension occurs in region IV between the yarn guide of PM ring and cop. Moreover, the variation of yarn tension increases especially at higher spindle speed, due to the vibration of yarn and PM ring.

Validation of yarn tension and maximum balloon form between measured and calculated values

In this section, the calculated yarn tensions are compared with measured ones for the regions I, II, and IV for spindle speed, of 5000–20,000 r/min. The measured and calculated maximum balloon diameters are also compared, according to spindle speed.

The difference—that is, the absolute error between the calculated and measured yarn tension—is presented in Figure 8 and in Appendix 3 for the spindle speeds of 5000–20,000 r/min.

The calculated and measured balloon forms are also illustrated in Figure 3, and the maximum balloon diameters are quantitatively compared in Table 3 for different spindle speeds. According to Figure 8 and Table 3, the difference between the calculated and measured

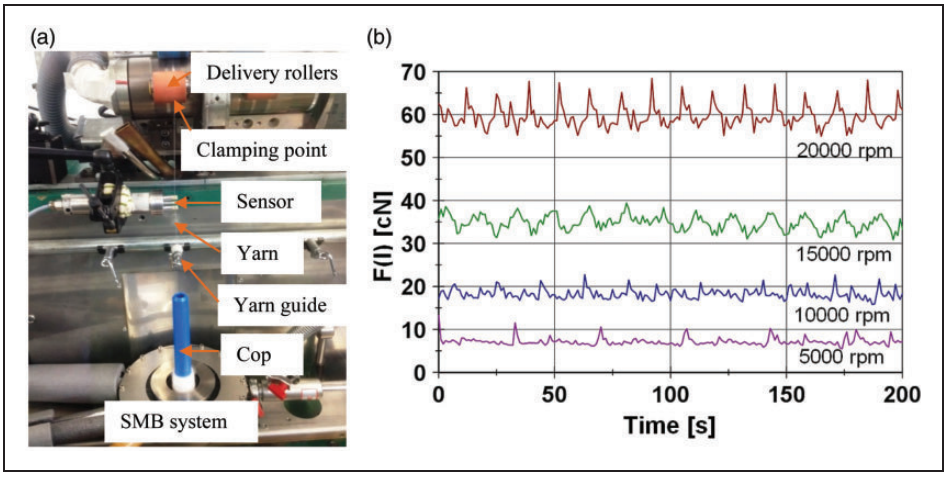

Figure 5. (a) Measurement set-up for yarn tension in region I between delivery rollers and yarn guide. (b) Mean values of yarn tension in region I at different spindle speeds.

yarn tension increases with spindle speeds higher than 15,000 r/min (Figure 8, Table 3). The errors can be attributed to the simplification of the assumptions in the model, such as considering the material behavior of the yarn as linear. Moreover, the induced vibrations of the PM and its influence on yarn are not considered in the model presented.

Conclusions and outlook

A theoretical model of the dynamic yarn path in the SMB ring spinning process was developed for the quasi-stationary case. The presented model was further modified based on the previous model of a ring traveler system. For this purpose, the equation of motion of the

Table 2. Experimental mean values of yarn tension at different regions with respect to spindle speeds

Spindle speed, r/min	Mean value of measured yarn tension					
	F(I), cN	Std. dev	F(II), cN	Std. dev	F(IV), cN	Std. dev
5000	7.0	0.9	6.8	0.1	11.8	1.4
10000	17.5	1.5	15.4	0.2	29.5	1.8
15000	35.4	1.8	30.0	0.3	58.5	2.8
20000	57.0	2.9	57.0	0.5	95.0	3.3

F(I): yarn tension between delivery rollers and yarn guide in region I; F(II): yarn tension between yarn guide and PM ring in region II; F(IV): yarn tension between PM ring and cop in region IV.

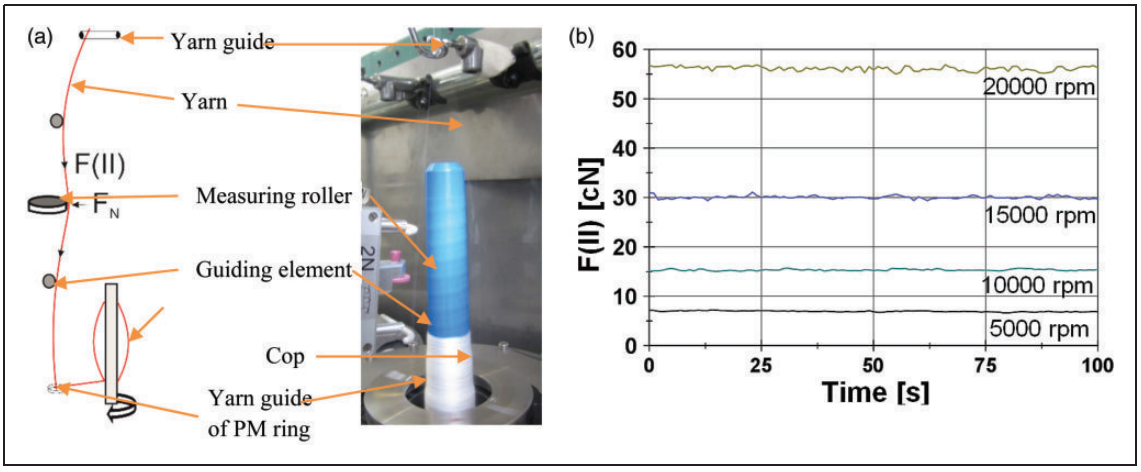

Figure 6. (a) Sketch[28] and experimental set-up of modified sensor used for the measurement of yarn tension in region II between the yarn guide and the yarn guide of the PM ring. (b) Mean values of yarn tension in region II at different spindle speeds. F (II): Yarn tension in region II; F_N: Radial component of the yarn tension.

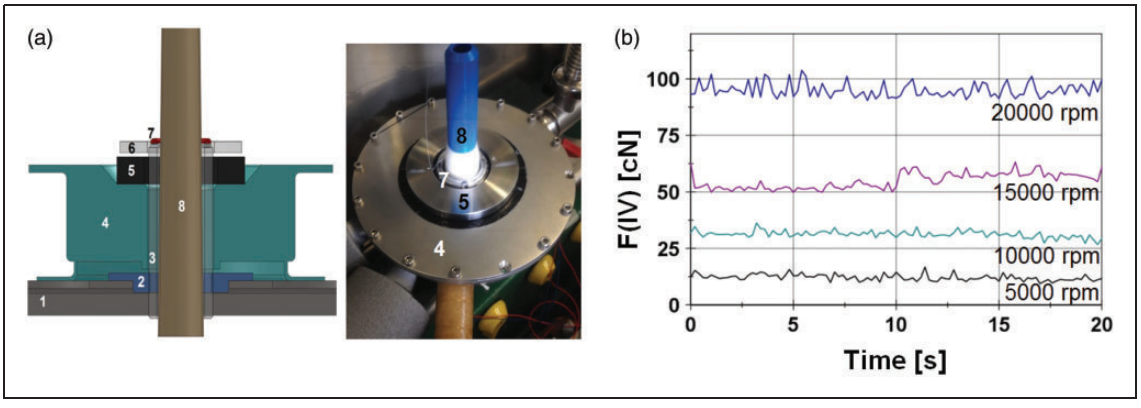

Figure 7. (a) Set-up for the measurement of yarn tension in region IV between the yarn guide of the PM ring and the cop. (b) Mean values of yarn tension in region IV at different spindle speeds. 1: ring rail; 2, 3: support for measuring ring; 4: cryostat; 5: permanent magnet ring; 6: superconductor; 7: measuring ring with spring leaves and strain gauges; 8: cop.

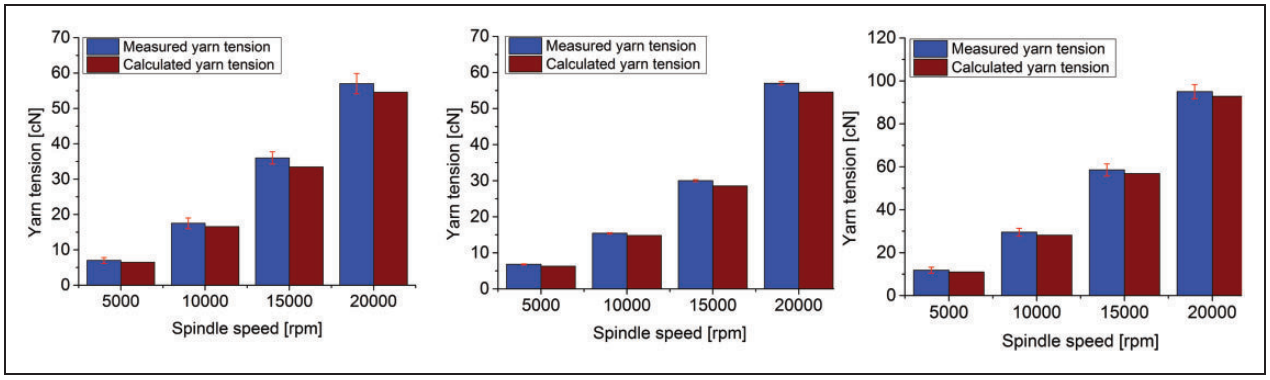

Figure 8. Comparison of yarn tension between measured and calculated values for (a) region I; (b) region II; (c) region IV.

Table 3. Comparison of maximum balloon diameter between calculated and measured values

Spindle speed (r/min)	Maximum calculated balloon diameter (Appendix 2) (mm)	Maximum measured balloon diameter (Table 1) (mm)	Absolute error (mm)
5000	45.4	45.7	0.3
10,000	54.0	54.5	0.5
15,000	59.8	60.8	1.0
20,000	67.4	68.7	1.3

rotating permanent magnet (PM) was at first described as a spring–mass–damper system. The necessary speed difference between the spindle and PM ring was derived with the damping parameter—that is, with the rotational decay constant for different spindle speeds. The equation of motion of the dynamic yarn path was presented in non-normalized values (with physical units). For numerical solution of the model, the equations were solved with the Runge-Kutta method, using the MATLAB program. The boundary conditions at the yarn guide of the PM ring were modified considering the dynamic behavior of the SMB system. The numerical results show the calculated yarn tension at different regions of the yarn path, and the corresponding balloon forms, according to spindle speed from 5000 to 20,000 r/min. The yarn tension and balloon form generally increase according to spindle speed, similar to the conventional spinning process.

In order to validate the developed model, the yarn tensions at different regions were also measured with modified sensors in consideration of the SMB spinning system, and the values were analyzed at different spindle speeds. A high speed camera was used to record the balloon forms with corresponding spindle speeds. The diameter of the recorded balloon form for each spindle speed was quantitatively analyzed with Image J software. Statistical analysis, such as for absolute error and standard deviation, for both the measured yarn tension and the balloon forms, showed a comparable correlation with the calculated values from the developed model. However, the experimental yarn tension was generally higher than the calculated value, especially at higher spindle speeds, because some assumptions, such as the vibration of PM ring during the spinning process and the resulting vibration of the yarn, were not considered in the mathematical model. The difference between the calculated and measured yarn tension at all regions increased due to the vibration of the PM, especially at higher spindle speed. Further, the friction between the yarn and the yarn guide of the PM were considered constant in the numerical solution, but they varied during the experiments. In further work, the vibration of the yarn and the PM ring needs to be considered in the numerical model, especially for higher spindle speeds. Moreover, the process parameters between the conventional and the SMB spinning system, for both the calculated and measured values, should be compared.

Declaration of conflicting interests

The authors declared no potential conflicts of interest with respect to the research, authorship, and/or publication of this article.

Funding

The authors disclosed receipt of the following financial support for the research, authorship, and/or publication of this article: This research is funded by German Research Foundation, DFG (Project No. CH 174/33-1 and SCHU 1118/12-1). The authors would like to thank DFG for the financial support.

References

1. Wulfhorst B, Gries T and Veit D. *Textile technology an introduction*. Munich: Carl Hanser Verlag, 2015.
2. Klein W. *The technology of short-staple pinning: Short-staple spinning series – Volume 1*. Manchester: The Textile Institute, 1998.

3. http://www.rieter.com/en/rikipedia/articles/technology-ofshort-staple-spinning/handling-material/winding-of-cops/effects-on-the-traveler/ (accessed 1 December 2015).
4. Hossain M, Abdkader A, Cherif C, et al. Innovative twisting mechanism based on superconducting technology for higher productivity in ring spinning machine. *Text Res J* 2014; 84: 871–880.
5. Cherif C, Abdkader A, Schultz L, et al. *Spooling and spinner device of a ring spinning frame or a ring twisting frame, and ring spinning and ring twisting method*. International Patent WO 2012/100964 A2, 2012.
6. Crank J. A theoretical investigation of cap and ring spinning systems. *Text Res J* 1953; 23: 266–276.
7. Mack C. Theory of the spinning balloon. *J Appl Math Mech* 1958; 11: 196–207.
8. De Barr AE. A descriptive account of yarn tensions and balloon shapes in ring spinning. *J Text Inst* 1958; 49: 58–88.
9. De Barr AE. The physics of yarn tensions and balloon shapes in ring spinning, winding and similar processes. *J Text Inst* 1960; 51: 17–38.
10. De Barr AE. The Role of Air Drag in Ring Spinning. *Journal of the Textile Institute Transactions* 1961; 52: 126–139.
11. De Barr AE and Catling H. The principles and theory of ring spinning. In: Charnley F and Harrison PW (eds) *Manual of cotton spinning*. Vol. 5, London: Butterworths Press, 1965.
12. Lisini GG, Toni P, Quilghini D, et al. A comparison of stationary and non-stationary mathematical models for the ring-spinning process. *J Text Inst* 1992; 83: 550–559.
13. Batra SK, Ghosh TK and Zeidman MI. An integrated approach to dynamic analysis of the ring spinning process, part I: without air drag and Coriolis acceleration. *Text Res J* 1989; 59: 309–317.
14. Batra SK, Ghosh TK and Zeidman MI. An integrated approach to dynamic analysis of the ring spinning process, part II: with air drag and Coriolis acceleration. *Text Res J* 1989; 59: 416–424.
15. Ghosh TK, Batra SK, Zeidman MI, et al. An integrated approach to dynamic analysis of the ring spinning process, part III: the effect of coefficient of friction and the balloon control rings. *Text Praxis Int* 1992; 47: 791–800.
16. Batra SK, Ghosh TK, Fraser WB, et al. An integrated approach to dynamic analysis of the ring spinning process, part IV: inherent instability of the free balloon. *Text Res J* 1995; 65: 417–423.
17. Fraser WB. On the theory of ring spinning. *Phil Trans Roy Soc Lond A* 1993; 342: 439–468.
18. Fraser WB. On unwinding yarn from a cylindrical package. *Phil Trans Roy Soc Lond A* 1992; 436: 479–498.
19. Tang ZX, Fraser WB and Wang X. Modelling yarn balloon motion in ring spinning. *Appl Math Model* 2007; 31: 1397–1410.
20. Tang ZX, Wang X and Fraser WB. Simulation and experimental validation of a ring spinning. *Sim Model Practice Theory* 2006; 14: 809–816.
21. Tang HD, Xu BG, Tao XM, et al. Mathematical modeling and numerical simulation of yarn behavior in a modified ring spinning system. *Appl Math Model* 2011; 35: 139–151.
22. Döbrich O, Gereke and Cherif C. Modelling of textile composite reinforcements on the micro-scale. *Autex Res J* 2014; 14: 28–33.
23. Hossain M, Telke C, Cherif C, et al. Mathematical modelling of the dynamic yarn path depending on spindle speed in a ring spinning process. *Textile Research Journal* , 2015. DOI: 10.1177/0040517515606355.
24. Buckel W and Kleiner R. *Superconductivity: fundamentals and applications*. Weinheim: Wiley, 2013 (in German).
25. Krabbes G, Fuchs G, Canders W-R, et al. *High temperature superconductor bulk materials: fundamentals, processing, properties control, application aspects*. Weinheim: Wiley, 2006.
26. Sparing M, Hossain M, Berger D, et al. Superconducting magnetic bearing as twist element in textile machines. *IEEE Trans Superconductivity* 2015; 25: 3600504/1–4.
27. Press WH, Flannery BP, Teukolsky SA, et al. *Numerical recipes: the art of scientific computing*. Cambridge: Cambridge University Press, 1986.
28. Hossain M, Abdkader A, Nocke A, et al. Measurement methods of dynamic yarn tension in a ring spinning process. *Fibres Text East Eur* 2016; 24: 36–43.
29. Image J. Image processing and analysis in JAVA. Available at: http://imagej.nih.gov/ij/ (accessed 15 March 2016).
30. Matthes A. *Analysis and simulation of yarn feed system in a circular knitting machines*. Dissertation, Technical University of Dresden, 2012.

Appendix 1

Process parameters for the numerical solution and experiments

Parameter	Value	Unit
Material	100% PES	()
Fiber count	1.14	(dtex) (g/10 km)
Staple length	38	(mm)
Roving count	499	(tex) (g/km)
Yarn count, m	20	(tex) (g/km)
Spindle speed, n_s	5000, 10,000, 15,000, 20,000	(r/min)
Delivery speed, v	7.1, 14.3, 21.4, 28.6	(m/min)
Twist	700	(T/m)
Balloon height, h	180	(mm)
Friction between yarn and yarn guide of PM ring, μ_y [30]	0.3	()
Mass of PM ring, m_{PM}	241 ± 1	(g)
Inner diameter of PM ring, a_{iPM}	43	(mm)
Outer diameter of PM ring, a_{aPM}	80	(mm
Moment of inertia of PM ring, J_R	248.5	(kg/mm^2)
Damping constant of PM ring, δ_{rot}	0.00137–0.00600	(s^{-1})

Appendix 2

Numerical results about yarn tension and balloon form

Exp.	Spindle speed	F(I)	F(II) (cN)	Balloon Parameter in region II (mm)		F(III)	F(IV)
()	(r/min)	(cN)	$h = 180$ (mm)	h_{max} (mm)	r_{max} (mm)	(cN)	(cN)
1	5000	6.5	6.3	163.9	22.7	6.4	11.0
2	10,000	16.6	14.8	129.6	27.0	16.0	28.1
3	15,000	33.5	28.5	121.7	29.9	32.2	56.9
4	20,000	54.6	54.5	114.9	33.7	52.4	92.8
5	25,000	78.7	60.2	106.5	41.2	75.2	133.8

F(I): yarn tension between the clamping point of delivery rollers and yarn guide; F(II): yarn tension between guide eye and yarn guide at PM; F(III): yarn tension at yarn guide of PM; F(IV): yarn tension between yarn guide of PM and winding point of cop; h: balloon height from yarn guide to the yarn guide of PM; r_{max}: maximum balloon diameter; h_{max}: balloon height from yarn guide to PM at r_{max}.

Appendix 3

Comparison of calculated values and measured mean values with absolute errors

Spindle speed (r/min)	F(I) (cN)			F(II) (cN)			F(IV) (cN)		
	Measured values	Calculated values	Absolute error	Measured values	Calulated values	Absolute error	Measured values	Calculated values	Absolute error
5000	7.0	6.5	0.5	6.8	6.3	0.5	11.8	11	0.8
10,000	17.5	16.6	0.9	15.4	14.8	0.6	29.5	28.1	1.4
15,000	35.4	33.5	1.9	30.0	28.5	1.5	58.5	56.9	1.6
20,000	57.0	54.6	2.4	57.0	54.5	2.5	95	92.8	2.2